Synthesis of Gradient Copolymers with Simultaneously Tailor-Made Chain Composition Distribution and Glass Transition Temperature by Semibatch ATRP: From Modeling to Application

Yin-Ning Zhou, Jin-Jin Li, Zheng-Hong Luo

Department of Chemical and Biochemical Engineering, College of Chemistry and Chemical Engineering, Xiamen University, Xiamen 361005, China
Correspondence to: Z.-H. Luo (E-mail: luozh@xmu.edu.cn)

Received 4 March 2012; accepted 3 April 2012; published online 28 April 2012
DOI: 10.1002/pola.26091

ABSTRACT: Recent studies have demonstrated that gradient copolymers exhibit unique thermal properties. Although these properties can be determined by copolymer composition, other factors such as chain and sequence lengths and their distributions can also influence them. Accordingly, the synthesis of gradient copolymers requires simultaneously tailor-made chain structure and thermal properties. In this work, we carried out a systematic study on the preparation of poly(methyl methacrylate-*grad*-2-hydroxyethyl methacrylate) [poly(MMA-*grad*-HEMA)] with synchronously tailor-made chain composition distribution and glass transition temperature (T_g) through semibatch atom transfer radical polymerization. First, a comprehensive model for simultaneously predicting gradient copolymer microstructure and T_g was presented using the concept of pseudo-kinetic rate coefficients and Johnston equation. The model was validated by comparing simulation results with the classical reference data. Furthermore, the model was used to guide the experimental synthesis of the poly(MMA-*grad*-HEMA) gradient copolymers potentially as excellent damping material. The thermal properties of these gradient copolymer samples were evaluated. © 2012 Wiley Periodicals, Inc. J Polym Sci Part A: Polym Chem 50: 3052–3066, 2012

KEYWORDS: computer modeling; copolymer composition distribution; glass transition temperature; kinetics (polym.); modeling; poly(MMA-*grad*-HEMA); semibatch atom tranfer radial polymerization (ATRP); thermal properties

INTRODUCTION Gradient copolymers are copolymers in which the instantaneous composition of the polymer changes continuously from one end of the chain to the other.[1,2] As a novel type of chain microstructures, synthesis of gradient copolymers, and evaluation of their materials properties have received increasing interest recently.[3–8] Both theoretical and experimental investigations have suggested that the composition distribution along chain can be an important microstructural parameter for fine-tuning nanomorphologies and thus physical and functional properties of polymer materials.[9–14] These investigations have also demonstrated that the gradual change in composition along the length of gradient copolymer chains results in less intrachain and interchain repulsion compared with block copolymers, lending to unique behaviors, especially unique thermal properties in bulk gradient copolymers.[2] For instance, Torkelson et al. have shown via differential scanning calorimetry (DSC) that unusually broad glass transition temperatures (T_gs) are present in strongly segregating styrene/4-hydroxystyrene (S/HS) gradient copolymers.[15] These properties of T_g are highly desirable in vibration and acoustic damping applications, which means that gradient copolymers are more excellent damping materials when compared with random and block copolymers.[16,17] Recent work from Torkelson et al. has indicated that these T_gs and glass transition breadths can be mainly tuned through the choice of monomer pairs and copolymer composition.[18] Besides, other factors such as chain and sequence lengths and their distributions can also influence T_g.[4,12,15] Therefore, when the gradient copolymers are applied in damping field, the synthesis of gradient copolymers requires simultaneously tailor-made chain composition and thermal properties.

The recent advent of controlled/living radical polymerization (CLRP) techniques makes the control of chain structure no longer a formidable task.[19–30] Among them, currently, some well established mechanisms are nitroxide mediated polymerization (NMP),[20,21] atom transfer radical polymerization (ATRP),[22–25] reversible addition fragmentation chain transfer polymerization (RAFT),[26,27] and single-electron transfer and single-electron transfer degenerative chain transfer living radical polymerization,[28–30] etc. They have been extensively exploited for the synthesis of a large variety of polymers

with predetermined molecular weight (MW) and narrow molecular weight distribution (MWD), as well as with well-defined block, star, graft, and brush architectures.[31] In general, introducing a comonomer in CLRP offers a possibility to prepare tailor-made copolymers with specific desired characteristics. However, in a batch process, composition drift is very common due to differences in the reactivity ratios of the monomers. To control copolymer composition, a semibatch operation is commonly used. It was experimentally and theoretically demonstrated that, through optimized feeding in a semibatch reactor, copolymers with uniform composition or linear gradient composition can be successfully designed and controlled.[21,32–37] In this field, Luo et al. have done excellent works.[33–37] For instance, they have developed a kinetic model for the semibatch RAFT copolymerization. The work theoretically demonstrated the feasibility of control of copolymer composition distribution in RAFT polymerization using semibatch-feeding policies.[33] This theoretical development was later extended to atom transfer radical copolymerization (ATRcoP). Nevertheless, this model did not consider the chain length dependence of termination rate coefficients for such polymerization, and also it was not validated via experiment.[34] But, it is undeniable that they carried out a systematic experimental study on the preparation of styrene/butyl acrylate (St/BA) copolymer products with various unprecedented chain microstructures through programmed semibatch RAFT copolymerization.[35,36] Recently, Ye et al.[38] developed a model with sequence lengths of chains and their distributions for RAFT copolymerization in semibatch operations using moment equations, Unfortunately, their model is not evaluated by any practical data and the idea of tailor-made materials properties such as T_g using chain and sequence lengths and their distributions is not reflected in their work. Wang et al.[21,32] introduced a computational tool based on kinetic Monte Carlo simulations for NMP that can generate recipes to synthesize copolymers with predesigned monomer sequences, but it also fails to predict any materials properties.

To simultaneously tailor-make chain composition and thermal properties/T_g, the chain composition and T_g equations must be solved synchronously. As described above, the models for the semibatch CLRP (including ATRP and RAFT polymerization) process have been deeply developed. Besides, there are also some models regarding T_g, especially the T_g of gradient copolymers. For instance, Hashimoto et al.[39] presented a mathematical model to predict the dynamic mechanical response for different spatial distributions of tapered block copolymers in 1983. The results showed that gradient copolymers could take the concept of tapered block copolymers one step further, with the tapered region extending along the entire length or the majority of the copolymer chain. Thus, one would expect more dramatic effects to be observed via dynamic mechanical testing of gradient copolymers. Fevotte et al.[40] suggested a model to predict/control the T_gs of free radical copolymers in 1998, whereas their model was failed to predict the chain structure due to the application of conventional free radical polymerization. Martin-Gomis et al.[41] investigated the T_g of copolymers based on dimethyl amino ethyl methacrylate and two structural hydroxy-functional acrylate isomers (HEMA and EHMA), along with the intramolecular and intermolecular structure and Johnston Equation, enabled a description of the experimental variations of the copolymer T_g. Liu et al.[42] proposed a equation to predict the T_g of sequence distribution-copolymers based on the extended Gibbs-DiMarzio equation in view of bond rotation flexibility and additivity of the corresponding stiff energies. More recently, Tonelli et al.[43] discussed the T_g of styrene/4-styrene copolymers with comonomer compositions and sequence distributions dependent conformational flexibilities of copolymers, as gauged by their conformational entropies. As a whole, the above models can be used to predict T_gs of different polymers including gradient copolymers, and thus the control of T_g is possible. Although they are only on T_g, it is possible to concurrently tailor-make chain composition and T_g when these T_g equations are incorporated/combined with the chain composition models.

In this work, we make effort to develop strategies through experiment and theoretical simulation approaches for the synthesis of gradient copolymers with simultaneously tailor-make chain composition and T_g. We use the preparation of poly(methyl methacrylate-*grad*-2-hydroxyethyl methacrylate) [poly(MMA-*grad*-HEMA)] through semibatch ATRP as an example for the work to obtain the poly(MMA-*grad*-HEMA) gradient copolymers potentially as excellent damping materials. In addition, in this work, we also evaluate the thermal properties (T_g) of these gradient copolymer samples and compare to the model prediction.

MODEL DEVELOPMENT

Polymerization Mechanism and Kinetic Equations for Semibatch ATRcoP

When the classical mechanism is applied to a specific ATRP system, some assumptions will be needed to simplify the model. In this work, the following assumptions, which have been proven to sufficient for describing the ATRP,[44] are applied: (1) the value of the rate constant for each step is independent on chain length, except the termination rate constant; (2) only chain transfer to monomer is considered; (3) the value of the initiator-activation rate constant is equal to that of the dormant. Therefore, the elementary reactions could be summarized in Table 1. Furthermore, for simplicity, in this work, we use a terminal model and also neglect some side reactions, such as thermal self-initiation and Propagation, *β-H* elimination by deactivator, which have been applied and proved in open reports.[34]

There are three types of chain species involved in the ATRcoP: (1) propagating radical chain ($P_{r,i}$·), (2) dormant radical chain ($P_{r,i}X$), and (3) dead chain (P_r). The subscript notation *r* denotes the length of chain, whereas *i* is the terminal unit of chain. For these species, the following molar balance equations (i.e., kinetic equations) in a batch reactor are summarized and listed in Table 2.

TABLE 1 Elementary Reactions Involved in ATRcoP

Type of reaction	Scheme
Initiation	$P_0X + C \overset{K_{eq}}{\longleftrightarrow} P_0\cdot + CX$
	$P_0\cdot + M_i \overset{k_{in,i}}{\longrightarrow} P_{1,i}\cdot$
Propagation	$P_{r,i}\cdot + M_j \overset{k_{p,ij}}{\longrightarrow} P_{r+1,j}\cdot$
ATRP equilibrium	$P_{r,i}X + C \overset{K_{eq}=k_a/k_{da}}{\longleftrightarrow} P_{r,i}\cdot + CX$
Transfer	$P_{r,i}\cdot + M_j \overset{k_{tr,ij}}{\longrightarrow} P_r + M\cdot$
Termination	$P_{r,i}\cdot + P_{s,j}\cdot \overset{k_{td,ij}}{\longrightarrow} P_r + P_s$
	$P_{r,i}\cdot + P_{s,j}\cdot \overset{k_{tc,ij}}{\longrightarrow} P_{r+s}$

Pseudo-Kinetic Rate Constants

Compared with homopolymerization, copolymerization involves more polymerization kinetic steps and requires more complex population balances. The mathematical treatment of copolymerization can be greatly simplified using the method of pseudo-kinetic constants developed by Hamielec in the early eighties.[45] Using the terminal model for copolymerization,[46] the equations for the pseudo-kinetic rate constants for propagation ($\overline{k_p}$), chain transfer ($\overline{k_{tr}}$), termination by disproportionation ($\overline{k_{td}}$), and termination by combination ($\overline{k_{tc}}$), are summarized in Table 3. In addition, Al-Harthi et al.[47] applied the pseudo-kinetic rate constant method to ATRcoP. In their work, they defined the pseudo-kinetic rate constants for activation and deactivation in ATRcoP equilibrium (i.e., $\overline{k_a}$ and $\overline{k_{da}}$), which are also summarized in Table 3.

In Table 3, three parameters must be defined. Among them, the mole fraction of polymer radical terminated in monomer of type i (ϕ_i) is given by:

$$\phi_i = \frac{[R_i]}{\sum_{j=1}^{N}[R_j]} \tag{1}$$

the mole fraction of monomer i in the monomer mixture (f_i) is given by:

$$f_i = \frac{[M_i]}{\sum_{j=1}^{N}[M_j]} \tag{2}$$

the molar fraction of dormant chains terminated in monomer i, (τ_i), is given by:

$$\tau_i = \frac{[D_i]}{\sum_{j=1}^{N}[D_j]} \tag{3}$$

Diffusion-Controlled Reactions

In free-radical polymerization, when the polymerization proceeds to intermediate and high conversions, the system becomes viscous and the reactants experience diffusion limitation, even though in the solution polymerization, it just delay the diffusion limitation.[35] Here, we use the free volume theory to describe the diffusion effect for all the reaction rate constants involved in this work.

During the polymerization, the free volume of the reaction mixture depends on the volume of the components present in the system. The total volume is calculated as:

$$v_f = \sum_{i=1}^{\#\text{ of components}} [0.025 + \alpha_i(T - Tg_i)]\frac{V_i}{V} \tag{4}$$

Chain-length dependence of reactions among large macromolecules is considered here by using different averages of the kinetic rate constant for such reactions. As shown in Table 1, only termination involves reaction between two large macromolecules. In addition, propagation, transfer between growing chain and catalyst, and transfer to small molecules involve reaction between a large and a small molecule, and a single average of the corresponding kinetic rate constant is adequate in those cases.[48] Accordingly, all the diffusion-controlled rate coefficients are summarized in Table 4.

TABLE 2 Kinetic Equations for Each Type of Chain Species

Type of chains	Mass balance equations
Propagating radical	$\frac{d[P_{r,i}\cdot]}{dt} = \sum_j k_{p,ij}[P_{r-1,j}\cdot][M_i] - \sum_j k_{p,ij}[P_{r,i}\cdot][M_j] + k_{a,i}[P_{r,i}X][C] - k_{da,i}[P_{r,i}\cdot][CX] - \sum_j k_{tr,ij}[P_{r,i}\cdot][M_j] - \sum_j\sum_s (k_{tc,ij} + k_{td,ij})[P_{r,i}\cdot][P_{s,j}\cdot]$
Dormant	$\frac{d[P_{r,i}X]}{dt} = k_{da,i}[P_{r,i}\cdot][CX] - k_{a,i}[P_{r,i}X][C]$
Dead	$\frac{d[P_r]}{dt} = \sum_j k_{tr,ij}[P_{r,i}\cdot][M_j] + \sum_i\sum_j\sum_{s=0}^{r} k_{tc,ij}[P_{r,i}\cdot][P_{r-s,j}\cdot] + \sum_i\sum_j\sum_{s=0}^{r} k_{td,ij}[P_{r,i}\cdot][P_{s,j}\cdot]$

TABLE 3 Definition for Various Pseudo-Kinetic Rate Constants

Type of reaction	Definition of pseudo-kinetic rate constants
Propagation	$\overline{k_p} = \sum_{i=1}^{N}\sum_{j=1}^{N} k_{p,ij}\phi_i f_i$
ATRP equilibrium	$\overline{k_a} = \sum_{i=1}^{N} k_{a,i}\tau_i$
	$\overline{k_{\mathrm{da}}} = \sum_{i=1}^{N} k_{\mathrm{da},i}\phi_i$
Transfer	$\overline{k_{\mathrm{tr}}} = \sum_{i=1}^{N}\sum_{j=1}^{N} k_{\mathrm{tr},ij}\phi_i f_i$
Termination	$\overline{k_{\mathrm{td}}} = \sum_{i=1}^{N}\sum_{j=1}^{N} k_{\mathrm{td},i,j}\phi_i\phi_j$
	$\overline{k_{\mathrm{tc}}} = \sum_{i=1}^{N}\sum_{j=1}^{N} k_{\mathrm{tc},ij}\phi_i\phi_j$

Method of Moments and Derivation of Moment Equations

The methodology used in this study is an extension of Zhu et al. work for ATRP.[48] The moments of chain species are summarized in Table 5.

With these moment definitions, the moment equations could be obtained by combining the moment definitions given in Table 5 with the population balance shown in Table 2 and the pseudo-kinetic rate constants shown in Table 3. A complete set of moment equations can be derived as summarized in Table 6. Therefore, one can readily describe the polymerization kinetics, such as monomer conversion (*Conv.*), cumulation copolymer composition (F_{cum}), number-average chain length (r_{n}), weight-average molecular chain length (r_{w}), polydispersity index (*PDI*), number-average molecular weight (*Mn*), and instantaneous copolymer composition (F_{inst}). Corresponding equations are as follows:

$$Conv. = \frac{\sum_{i=1}^{N}(M_{i0} - M_{is} - M_{ir})}{\sum_{i=1}^{N} M_{i0}} \tag{5}$$

$$F_{cum} = \frac{M_{i0} - M_{is} - M_{ir}}{\sum_{i=1}^{N}(M_{i0} - M_{is} - M_{ir})} \tag{6}$$

$$r_n = \frac{\sum_i\left(\lambda_i^1 + \mu_i^1 + \tau^1\right)}{\sum_i\left(\lambda_i^0 + \mu_i^0 + \tau^0\right)} \tag{7}$$

$$r_w = \frac{\sum_i\left(\lambda_i^2 + \mu_i^2 + \tau^2\right)}{\sum_i\left(\lambda_i^1 + \mu_i^1 + \tau^1\right)} \tag{8}$$

$$PDI = \frac{r_w}{r_n} \tag{9}$$

$$M_n = \sum_i^N r_n F_{cum}\overline{M_{n,i}} \tag{10}$$

$$F_{inst} = \frac{\sum_j k_{p,ji}\mu_j^0[M_i]}{\sum_i\sum_j k_{p,ji}\mu_j^0[M_i]} \tag{11}$$

Semibatch Reactor Model

A reactor model for the semibatch polymerization must be developed due to the control of the composition distribution along the chain. In addition, in this work, a well-mixed isothermal tank reactor is assumed. Furthermore, due to a trace amount of initiator and a constant volume of solvent, only monomer and polymer significantly contribute to volume (V) and density (ρ) in the semibatch operation process. Therefore, in the semibatch reactor, the mass balance equations for all entities can be worked out.

For the semibatch reactor, the evolution of reaction volume V can be derived:

$$\frac{dV}{dt} = V_f - \sum_{i=1}^{n}\overline{M_{n,i}}R_{p,i}V\left(\frac{1}{\rho_p} - \frac{1}{\rho_i}\right) \tag{12}$$

The evolution of density in the reactor can be obtained via applying mass balance to all entities:

$$\frac{d(V\rho)}{dt} = V_f\rho_f \tag{13}$$

$$\text{i.e.,}\ \frac{d\rho}{dt} = \frac{V_f\rho_f}{V} - \frac{\rho}{V}\frac{dV}{dt} \tag{14}$$

TABLE 4 The Expression for Diffusion-Controlled Rate Coefficients

Type of reaction	Diffusion-controlled rate coefficients
Propagation	$\langle k_{\mathrm{p}}\rangle = \overline{k_{\mathrm{p}}}\exp\left[-B_{\mathrm{p}}\left(\frac{1}{v_{\mathrm{f}}} - \frac{1}{v_{\mathrm{f0}}}\right)\right]$
ATRP equilibrium	$\langle k_{\mathrm{a}}\rangle = \overline{k_{\mathrm{a}}}\exp\left[-B_{\mathrm{a}}\left(\frac{1}{v_{\mathrm{f}}} - \frac{1}{v_{\mathrm{f0}}}\right)\right]$
	$\langle k_{\mathrm{da}}\rangle = \overline{k_{\mathrm{da}}}\exp\left[-B_{\mathrm{da}}\left(\frac{1}{v_{\mathrm{f}}} - \frac{1}{v_{\mathrm{f0}}}\right)\right]$
Transfer	$\langle k_{\mathrm{tr}}\rangle = \overline{k_{\mathrm{tr}}}\exp\left[-B_{\mathrm{tr}}\left(\frac{1}{v_{\mathrm{f}}} - \frac{1}{v_{\mathrm{f0}}}\right)\right]$
Termination	$\langle k_{\mathrm{td}}\rangle = \overline{k_{\mathrm{td}}}\left(\frac{r_{\mathrm{n}}}{r_{\mathrm{w}}}\right)^{x/2}\exp\left[-B_{\mathrm{td}}\left(\frac{1}{v_{\mathrm{f}}} - \frac{1}{v_{\mathrm{f0}}}\right)\right]$
	$\langle k_{\mathrm{tc}}\rangle = \overline{k_{\mathrm{tc}}}\left(\frac{r_{\mathrm{n}}}{r_{\mathrm{w}}}\right)^{x/2}\exp\left[-B_{\mathrm{tc}}\left(\frac{1}{v_{\mathrm{f}}} - \frac{1}{v_{\mathrm{f0}}}\right)\right]$

TABLE 5 Definition of Various Chain Moments

Type of chains	Definition of the moments
Propagating radical	$\mu_i^m = \sum_{i=1}^{\infty} i^m [P_{r,i}\cdot]$
Dormant	$\lambda_i^m = \sum_{i=1}^{\infty} i^m [P_{r,i}X]$
Dead	$\tau^m = \sum_{i=1}^{\infty} i^m [P_r]$

In addition, for the *i*th species in the semibatch reactor, the following mass balance equation can be derived:

$$\frac{d(VC_i)}{dt} = V_f C_{if} + VR_i \tag{15}$$

$$\frac{dC_i}{dt} = \frac{1}{V}\left(V_f C_{if} - C_i \frac{dV}{dt}\right) + R_i \tag{16}$$

Glass Transition Temperature Model

For control purposes, a satisfactory model should satisfy an acceptable compromise between simplicity and accuracy of the predictions. In this work, the instantaneous T_g is calculated using the Johnston equation,[49] which can be considered as an extension of the earlier work of Fox.[50] The selected instantaneous T_g model can predict T_g in terms of monomer unit sequences (dyad sequences) in a copolymer with assuming that M_1M_1, M_1M_2 or M_2M_1, and M_2M_2 dyads have their own T_gs. Accordingly, the overall T_g of a copolymer can be described as follows:

$$\frac{1}{Tg(t)} = \frac{w_1(t)P_{11}(t)}{Tg_{11}} + \frac{w_2(t)P_{22}(t)}{Tg_{22}} + \frac{w_1(t)P_{12}(t) + w_2(t)P_{21}(t)}{Tg_{12}} \tag{17}$$

TABLE 6 Differential Moment Equations

Zeroth order moments	Propagating radical chains	$\frac{d\mu_0}{dt} = \langle k_a\rangle[C][\lambda_0] - \langle k_{da}\rangle[CX][\mu_0] - \langle k_{tr}\rangle[M][\mu_0] - (\langle k_{tc}\rangle + \langle k_{td}\rangle)[\mu_0][\mu_0]$
	Dormant chains	$\frac{d\lambda_0}{dt} = -\langle k_a\rangle[C][\lambda_0] + \langle k_{da}\rangle[CX][\mu_0]$
	Dead chains	$\frac{d\tau_0}{dt} = \langle k_{tr}\rangle[M][\mu_0] + \langle k_{td}\rangle[\mu_0][\mu_0] + \frac{\langle k_{tc}\rangle}{2}[\mu_0][\mu_0]$
First-order moments	Propagating radical chains	$\frac{d\mu_1}{dt} = \langle k_a\rangle[C][\lambda_1] - \langle k_{da}\rangle[CX][\mu_1] + \langle k_p\rangle[M][\mu_0] - \langle k_{tr}\rangle[M][\mu_1] - (\langle k_{tc}\rangle + \langle k_{td}\rangle)[\mu_0][\mu_1]$
	Dormant chains	$\frac{d\lambda_1}{dt} = -\langle k_a\rangle[C][\lambda_1] + \langle k_{da}\rangle[CX][\mu_1]$
	Dead chains	$\frac{d\tau_1}{dt} = \langle k_{tr}\rangle[M][\mu_1] + \langle k_{td}\rangle[\mu_0][\mu_1] + \langle k_{tc}\rangle[\mu_0][\mu_1]$
Second-order moments	Propagating radical chains	$\frac{d\mu_2}{dt} = \langle k_a\rangle[C][\lambda_2] - \langle k_{da}\rangle[CX][\mu_2] + \langle k_p\rangle[M][\mu_0] + 2\langle k_p\rangle[M][\mu_1] - \langle k_{tr}\rangle[M][\mu_2] - (\langle k_{tc}\rangle + \langle k_{td}\rangle)[\mu_0][\mu_2]$
	Dormant chains	$\frac{d\lambda_2}{dt} = -\langle k_a\rangle[C][\lambda_2] + \langle k_{da}\rangle[CX][\mu_2]$
	Dead chains	$\frac{d\tau_2}{dt} = \langle k_{tr}\rangle[M][\mu_2] + \langle k_{td}\rangle[\mu_0][\mu_2] + \langle k_{tc}\rangle[\mu_0][\mu_2] + \langle k_{tc}\rangle[\mu_1][\mu_1]$
Small molecules	Monomers	$\frac{dM}{dt} = -(\langle k_p\rangle + \langle k_{tr}\rangle)[M][\mu_0]$
	Activator	$[C] = [C_0] - [CX] = \frac{d[C]}{dt} = -\langle k_a\rangle[C][\lambda_0] + \langle k_{da}\rangle[CX][\mu_0]$
	Deactivator	$[CX] = [P_0X] - [\lambda_0]$
		$\frac{d[CX]}{dt} = -\frac{d[C]}{dt}$

TABLE 7 Kinetic Rate Constants of the MMA/HEMA-TMS ATRcoP used in Simulation[a]

Parameter	Value	Ref.
k_{p11} (L/mol ·s)	$10^{6.427}$ exp (−22360/RT)	51
k_{p22} (L/mol ·s)	$10^{6.954}$ exp (−21900/RT)	52
k_{tc11} (L/mol ·s)	1.0×10^7	53
k_{tc22} (L/mol ·s)	$0.9k_{t2} = 0.99 \times 10^6$	54
k_{td11} (L/mol ·s)	$k_{tc11} \times 2.43 \times 10^3$ exp (−15460/T)	53
k_{td22} (L/mol ·s)	$0.1k_{t2}$	54
k_{t11},k_{t21} (L/mol ·s)	$(k_{t11} \times k_{t22})^{1/2}$	55
r_1	0.86	56
r_2	0.66	56
t_{tr11} (1/s)	0.0198	Set to an arbitrary low value
t_{tr22} (1/s)	0.0122	Set to an arbitrary low value
t_{tr12}, t_{tr21} (1/s)	$(k_{tr11} \times k_{tr22})^{1/2}$	Use the same method as k_t
k_{a1} (L/mol · s)	0.6035[b]	This work
k_{a2} (L/mol · s)	0.5767[b]	This work
k_{da1} (L/mol · s)	0.2518×10^{7}[b]	This work
k_{da2}	3.2231×10^{7}[b]	This work

[a] HEMA-TMS(use parameters of HEMA by analogy)

[b] Obtained by experimental data fitting.

where, T_{g11} and T_{g22} are the T_g of the homopolymers, T_{g12} or T_{g21} is the T_g of an ideally alternating copolymer. Namely, $T_{g12} = T_{g21}$,[40] w_i is the instantaneous weight fraction of monomer i in the copolymer, $P_{ij(t)}$ *is the dyad distribution and can be defined via eqs 18 and 19:*

$$\frac{1}{P_{ij}(t)} = 1 + r_i \frac{[M_i(t)]}{[M_j(t)]} \qquad (i = 1 \text{ or } 2,\ \mathrm{i} \neq \mathrm{j}) \tag{18}$$

$$P_{ii}(t) = 1 - P_{ij}(t) \qquad (i = 1 \text{ or } 2,\ \mathrm{i} \neq \mathrm{j}) \tag{19}$$

where, r_i is the well known free radical polymerization reactivity ratio, $[M_i(t)]$ is the instantaneous concentration of monomer *i.*

When using the above model to predict the breadth of T_g, we defined $\triangle T_g$ as follow:

$$\Delta Tg = Tg_{11} - Tg(t) \quad \text{(in normal mode)} \tag{20}$$

$$\Delta Tg = Tg(t) - Tg_{22} \quad \text{(in inverse mode)} \tag{21}$$

Model Implementation and Estimation of Model Parameters

Equations 1–19 and equations described in Tables 2–6 constitute the integrated model, which can be used to predict concurrently chain composition and T_g. In addition, these equations include a set of stiff and ordinary differential equations. The ode23s-function, based on a modified

TABLE 8 Materials Properties for the MMA/HEMA-TMS ATRcoP[a]

Parameter	Value	Ref.	Parameter	Value	Ref.
ρ_{m1} (g/cm^3)	$0.9569–1.2129 \times 10^{-3}$ (T − 273.15)	57	Tg_{p1} (K)	387	53
ρ_{m2} (g/cm^3)	0.929 (1.073)	54	Tg_{p2} (K)	328	54
ρ_p (g/cm^3)	1.15	54	Tg_{m1} (K)	167	53
α_{p1} (1/K)	0.00048	53	Tg_{m2} (K)	213	54
α_{p2} (1/K)	0.000075	54	Tg_S (K)	115	58
α_{m1} (1/K)	0.001	53	B_p (dimensionless)	0.65 ± 0.32	48
α_{m2} (1/K)	0.0005	54	B_t (dimensionless)	6.64 ± 0.75	48
α_p (1/K)	$F_{cum1}\ \alpha_{p1} + F_{cum2}\ \alpha_{p2}$	59	B_{tr} (dimensionless)	0.5	48
α_S (1/K)	0.00107	60	B_a (dimensionless)	5.0 ± 0.023	48
Tg_p	$1/Tg_p = w_1\ P_{11}/Tg_{p1} + w_2 P_{22}/Tg_{p2} + (w_1 P_{12} + w_2\ P_{21})/Tg_{p12}$	49	B_{da} (dimensionless)	3.0 ± 0.41	48

[a] All the properties of HEMA-TMS are similar to HEMA's

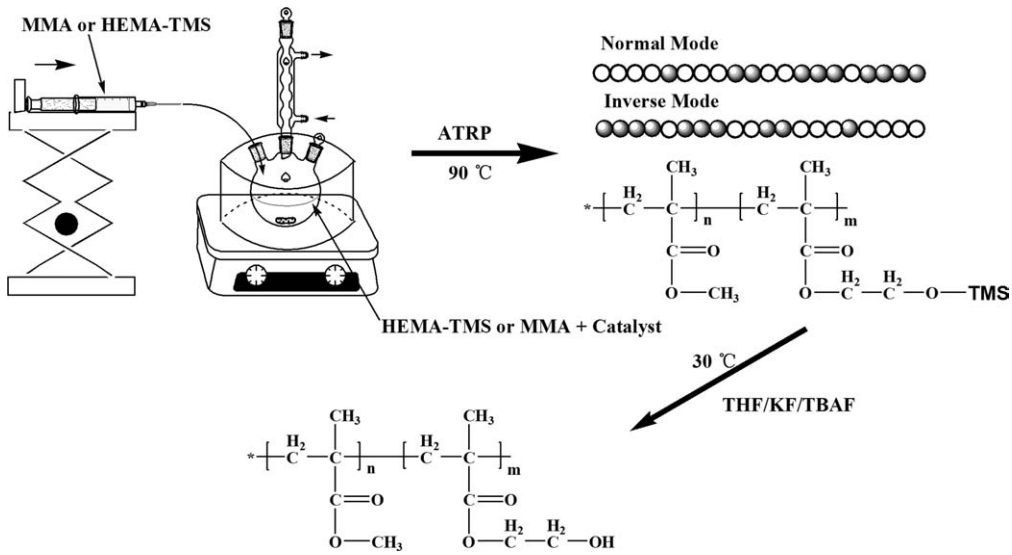

SCHEME 1 Experimental apparatus for the semibatch ATRP.

Rosenbrock formula of second-order, provided in MATLAB 7.0 software was used to solve the ordinary differential equations.

To solve the above model, some kinetic, thermodynamic, and property parameters related to the model must be obtained in advance. The main parameters and their values applied in this work are listed in Tables 7 and 8.

EXPERIMENTAL

Materials

Methyl methacrylate (MMA, 98%) was supplied by Sinopharm Chemical Reagent (SCRC) and was rinsed with 5 wt % aqueous NaOH solution to remove the inhibitor. 2-Hydroxyethyl methacrylate (HEMA, 95%) and Tetrabutylammonium fluoride (TBAF, 1M in tetrahydrofuran) were obtained from TCI (Shanghai) Development. HEMA was purified by washing an aqueous solution of monomer with hexane to remove ethylene glycol dimethacrylate, salting the monomer out of the aqueous phase by addition of NaCl, drying over $MgSO_4$, and distilling under reduced pressure. Ethyl 2-bromoisobutyrate (Eib-Br, 98%) were obtained from A Better Choice for Research Chemicals GmbH & Co. KG. (ABCR). 4,4′-Dinonyl-2,2′-bipyridyl (dNbpy, Nanjing Chemzam Pharmtech, 99%) was recrystallized three times from ethanol. CuBr (SCRC, 99%) was purified by washing it with acetic acid and methanol alternatively three times, and dried under vacuum at 45 °C for 24 h. Potassium fluoride (KF, 99%, SCRC) was used as received. All other reagents and solvents were obtained from SCRC and used without further purification.

Synthesis of HEMA-TMS

Due to poor solubility of HEMA in low polar solvents, HEMA was often polymerized in its protected form, 2-(trimethylsilyl)-ethyl methacrylate (HEMA-TMS). The resulting polymers were more compatible with organic media, especially when used for the synthesis of block copolymers followed by deprotection to make amphiphilic materials or homopolymerized then followed by a transesterification with 2-bromoisobutyryl bromide to subsequently prepare graft copolymers, leading to polymer brushes.[61] The detailed synthesis procedure of HEMA-TMS can be found in Ref. 62.

Synthesis of MMA/HEMA-TMS Random, Diblock, and Gradient Copolymers

The gradient copolymers were synthesized through semibatch ATRP described in Scheme 1. A typical procedure can be described as follows: Toluene, CuBr, $CuBr_2$, dNbpy, and MMA or HEMA-TMS were first added to a dried round-bottom flask, and the mixture was degassed three times by freeze/pump/thaw cycles. In addition, in another reaction flask, CuBr, $CuBr_2$, dNbpy and HEMA-TMS, or MMA were added and degassed by three freeze/pump/thaw cycles. After stirring the mixtures for 30 min, the primary flask was placed in a preheated oil bath at 90 °C, and the initiator Eib-Br was added. The secondary reaction mixture was transferred into an airtight syringe and assembled to a syringe pump. Synchronously, the continuous addition of the secondary reaction mixture to the primary one was started at a model optimized rate, which corresponds to targeted monomer conversion. Samples were taken of about 0.1–0.2 mL every 1.5 h. After 6.5 h, the HEMA-TMS or MMA addition was complete. The reaction was stopped after 7 h by cooling the flask to room temperature and exposing the reaction mixture to air.

Random copolymers were made using batch ATRP with Eib-Br as initiator. The monomers, solvent, and catalyst system were combined in a dried round-bottom flask, and the mixture was degassed three times by freeze/pump/thaw cycles. After stirring the mixtures for 30 min, the primary flask was placed in a preheated oil bath at 90 °C, and the initiator Eib-Br was added with an injector under N_2. After 7 h, the flask was removed from the oil bath and allowed to cool to room temperature.

Diblock copolymers were synthesized using sequential, batch ATRP. The PMMA macroinitiator was first synthesized in

TABLE 9 Recipes for all the Experimental Studies

Expt.		MMA mmol (mL)	HEMA-TMS mmol (mL)	Initiator (mmol)	CuBr (mmol)	$CuBr_2$ (mmol)	dNbpy (mmol)	Solvent (mL)	V_f (mL h^{-1})
1	r. f.	30.98 (3.3)		0.12	0.09	0.0046	0.18	1.07	
	a. s.		34.08 (7.1)		0.10	0.0051	0.20	2.5	1.52
2	r. f.	30 (3.2)		0.12	0.087	0.00435	0.174	2	
	a. s.		24 (5)		0.07	0.0035	0.14	1.5	1.00
3	r. f.		24 (5)	0.12	0.07	0.0035	0.14	1.5	
	a. s.	30 (3.2)			0.87	0.00435	0.174	2	0.80
4	r. f.	30 (3.2)	24 (5)	0.12	0.157	0.00785	0.314	3.5	
5	r. f.		24 (5)	0.12	0.07	0.0035	0.14	3.5	

r. f., reactive flask; a. s., airtight syringe.

toluene with Eib-Br as initiator. Then, the macroinitiator, solvent, and catalyst system were combined in a dried round-bottom flask; the flask was degassed three times by freeze/pump/thaw cycles. After three repetitions, a predetermined amount of HEMA-TMS was added with an injector under N_2. The flask was placed in a preheated and thermally regulated oil bath at 90 °C. After 7 h, the reaction was stopped.

All of the above polymer solutions were diluted with $CHCl_3$ and passed over an alumina column to remove the catalyst. The solvent was distilled off under vacuum using a rotary evaporator at 25 °C, and then the polymer was precipitated in petroleum ether, finally dried under vacuum for 24 h. Monomer conversion was measured by gravimetry. Recipes for all the experimental studies were listed in Table 9 (Expt. 2 and 3 were used to synthesize the polymer with linear gradient and inverse linear gradient composition, respectively; Expt. 4 and 5 were for synthesizing the random and biblock copolymers, respectively).

The overall ratio of incorporated monomer in resulting copolymer was determined using ^{1}H-NMR (Fig. 1, taking linear gradient copolymer for example) measurements by comparing the peak area ratio of characteristic signals for PMMA (3.4 ppm, 3H, —O—$\mathbf{CH_3}$) and PHEMA-TMS (3.94 ppm, 2H, —$\mathbf{CH_2}$—OCO—, and 3.62 ppm, 2H, —$\mathbf{CH_2}$—O—Si$(CH_3)_3$; 0.05–0.16 ppm, 9H, —Si$\mathbf{(CH_3)_3}$).

Preparation of MMA/HEMA Random, Diblock, and Gradient Copolymers

Each kind of copolymer (2 g) was dissolved in 50 mL of dry THF. KF (100 mg, 1.64 mmol) and TBAF (164μl, 0.164 mmol) were added to the polymer solution and stirred for 24 h at room temperature. A part of solvent was evaporated under reduced pressure, and the polymer was precipitated in water. After filtration, the polymer was dried under vacuum for 24 h, and the copolymer of MMA and HEMA was obtained. The ^{1}H-NMR (Fig. 1) result indicated that the TMS group on the copolymer was fully removed [absence of TMS—O— resonance $\delta = 0.05$–0.16 ppm, 9H, —Si$\mathbf{(CH_3)_3}$].

Measurements

The copolymer compositions were determined by nuclear magnetic resonance (^{1}H-NMR) spectroscopy (Bruker AV400 MHz) in dimethyl sulfoxide-d_6. To obtain the relative amounts of the comonomers incorporated in polymer chains were estimated from the areas under assigned peaks of the spectra. The copolymer composition was determined by comparing the integrated intensities of these resonance signals as above mention.

The molecular weight (Mn) and molecular weight distribution (Mw/Mn, PDI) of the polymer was determined at 40 °C by gel permeation chromatography (GPC) equipped with a waters 1515 isocratic HPLC pump, three Styragel columns (Waters HT4, HT5E, and HT6) and a waters 2414 refractive index detector (set at 30 °C), using THF as the eluent at the flow rate of 1.0 mL min^{-1}. A series of poly(methyl methacrylate) (PMMA) narrow standards were used to generate a universal calibration curve.

The thermal analysis of the MMA/HEMA copolymers was carried out using a differential scanning calorimeter (Netzsch DSC 204). Cooling was accomplished by a liquid nitrogen-cooling accessory. Around 10 mg of sample was loaded into an aluminum pan with an empty pan serving as a reference. The dry nitrogen was purged into the DSC cell with a flow rate of 50 mL min^{-1}. The samples were first heated at a rate of 10 °C min^{-1} to 150 °C and held at constant temperature for 5 min to eliminate thermal history. The samples were then quenched at a rate of −40 °C min^{-1} to 0 °C before being reheated to 150 °C at a rate of 10 °C min^{-1}. All data associated with glass transition measurements were obtained from the second heating scan.

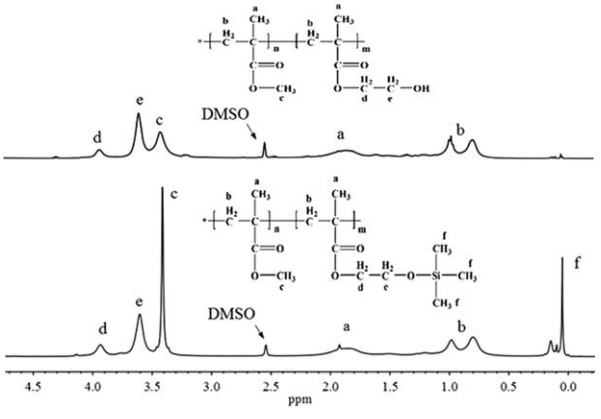

FIGURE 1 ^{1}H-NMR spectrum of the MMA/HEMA and MMA/HEMA-TMS linear gradient copolymers.

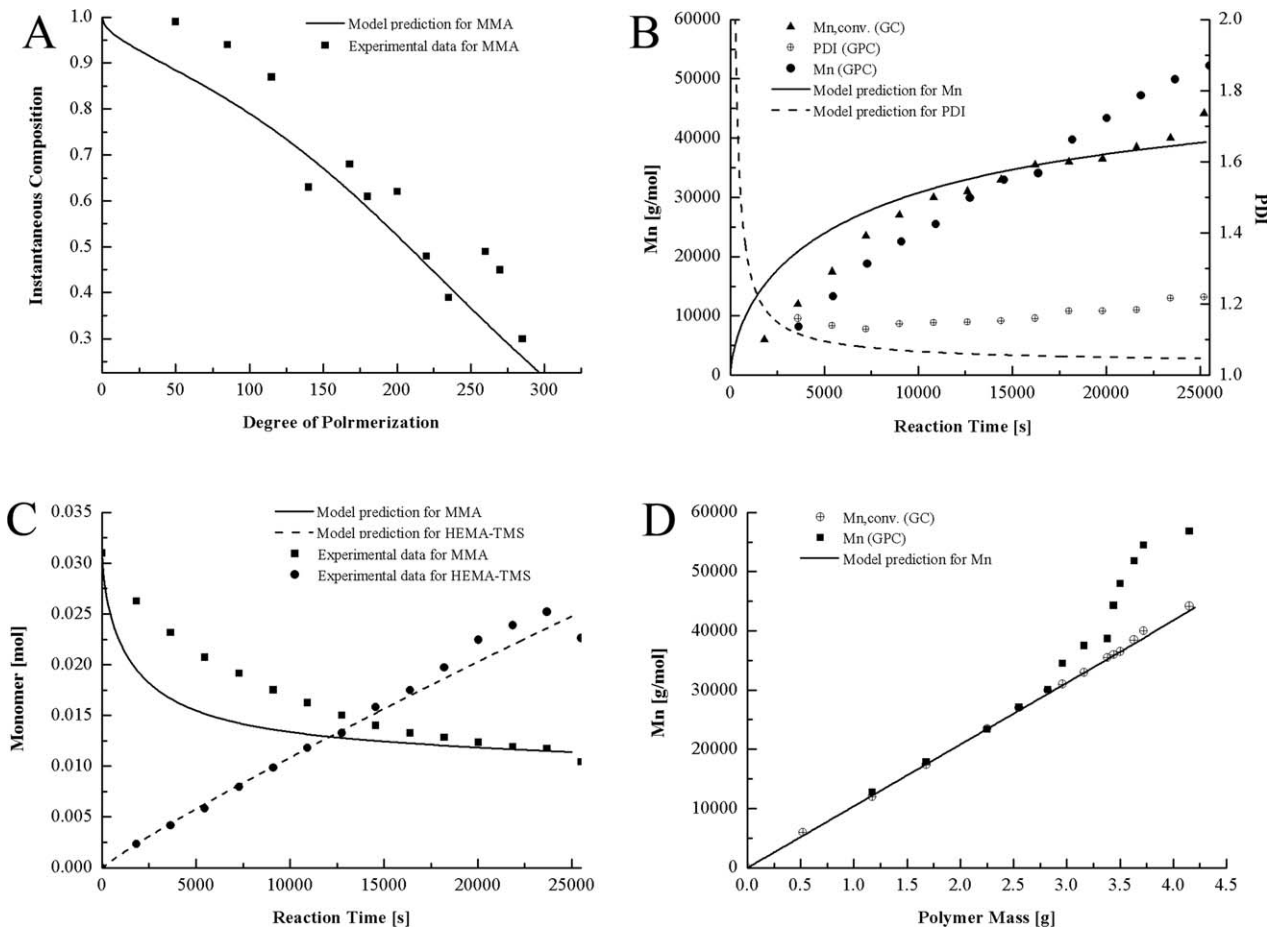

FIGURE 2 Comparison between model predictions and experimental data from classical literature (Ref. 63) for the semibatch ATRP for producing linear gradient copolymers: A instantaneous composition of poly(MMA-*grad*-HEMA-TMS) versus degree of polymerization, B molecular weight and polydispersity index versus reaction time, C monomer concentration versus reaction time, D molecular weight versus polymer yield based on monomer conversion.

RESULTS AND DISCUSSION

Model Validation

To validate the model developed above for the semibatch reactor, the simulation results were first tested against experimental data recorded in Matyjaszewski and coworkers report.[63] In that report, the experimental conditions are as follows: the ATRcoP of MMA and HEMA-TMS at 90 °C in a semibatch reactor, which corresponds to Expt. 1 described in Table 9. In addition, due to the absence of the activating and deactivating rate constants for our studied system in open reports, they are estimated via the least-square method based on the experimental data reported in Refs. 62 and 64 and the estimated values are listed in Table 7. Moreover, the adjustable free volume parameters used in the diffusion-controlled rate coefficients equations are difficult to estimate. These used adjustable parameters were directly available from the literature for similar system.[48] The results show that such approximation is acceptable. By substituting the model parameters described in Tables 7 and 8 for related terms in the above model, respectively, the simulated results were obtained and shown in Figure 2.

From Figure 2, one can know that the compared parameters include instantaneous composition, monomer concentration, molecular weight, and polydispersity index. Namely, Figure 2(A) shows that the instantaneous composition of MMA mole faction decreases continuously with an average polymer chain from 1 in the beginning of chain to 0.23 at the end. The deviation between experimental data and the simulated data is due to the slow initiator decomposition rate. The results confirm the synthesis of a gradient structure. Figure 2(B) illustrates the evolution of molecular weight (Mn) and PDI during gradient copolymerization. Figure 2(C) shows that the evolution of monomer concentration during the gradient copolymerization. Fast consumption of MMA can be observed during the early stage of the polymerization as a result of a high initiator concentration and a low concentration of competing HEMA-TMS. During the polymerization process, the rate of consumption of MMA slows down due to a dilution of MMA with increasing amount of HEMA-TMS. The prediction for the MMA concentration deviates from experimental data at the initial time owe to the conditions of simulation, which are more ideal than actual operation. In addition, Figure 2(D) indicates the molecular

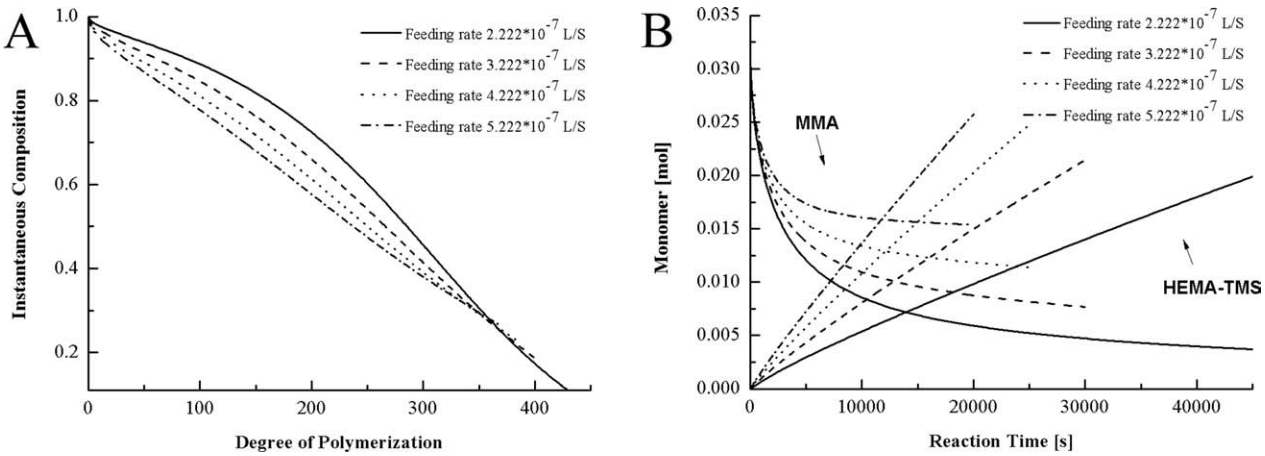

FIGURE 3 Effect of monomer feeding rate on instantaneous composition of poly(MMA-*grad*-HEMA-TMS) (A) and monomer concentration (B) at semibatch ATRP process.

weights (Mn) versus polymer yield based on monomer conversion. The model prediction for Mn tracks the experimental data of theoretical molecular weight closely and the linear increase of Mn with polymer mass indicates a constant number of chains. From Figure 2(B and D), the deviation between Mn (GPC) and Mn, conv (GC) can be observed after 3 h, when the polymer mass is about 3 g. As explained by Matyjaszewski and coworkers,[63] the decrease of the overall MMA to HEMA-TMS ratio in the formed copolymer results in an increasingly different behavior of the copolymer in comparison to narrow PMMA standards. For PDI, the model captures the trend. The deviation from the simulation at high conversion (at long reaction time) can be explained by the ideal conditions of simulation based on some assumptions, which is needed to simplify the model.

As a whole, Figure 2 illustrates the comparisons between the experimental and simulated data at the semibatch polymerization condition, which shows a good agreement between the experimental data and the simulated results. It means that the semibatch model can be utilized for further simulation study. Next, the above model will be used to predict the effect of the feeding rate of HEMA-TMS on the gradient copolymer composition to guide for synthesizing the linear gradient copolymers.

Model Application

As mentioned previously, the semibatch operation is the best methodology for synthesizing the gradient copolymer. The gradient copolymerization process is influenced by two important parameters. First, the monomer addition rate, it affects the kinetics, thereby affecting the conversion and then the structure of polymer chain. Indeed, if monomer addition is faster than monomer consumption, it will result in the decrease of conversion. Second, the choice of added monomer is also one of important parameters. Working with two monomers characterized by different reactivity ratios, it is essential to add the more reactive monomer to force the incorporation of this monomer in the macromolecular chains to form a specific gradient molecular structure. Herein, we use the above model to predict their effects on gradient copolymerization.

Effect of the Feeding Rate on Gradient Copolymer Composition in Semibatch Process

First, the effects of four different feeding rates on instantaneous copolymer composition and monomer concentration are simulated via the above model. During the simulation, we have adopted the same experimental conditions done by Matyjaszewski and coworkers.[63]

The simulated results are shown in Figure 3. From Figure 3(A), all the instantaneous compositions of MMA decrease continuously with the increase of average polymer chain at different feeding rate. In addition, with the increase of feeding rate, the curve for instantaneous composition becomes closely to linear. Figure 3(B) shows that, both the two-monomer conversions decrease with the increase of feeding rate. However, when the feeding rate greatly exceeds the rate of consumption for HEMA-TMS, a dilution of MMA will happen, which is attributed to the accumulation of HEMA-TMS in the system. However, the decrease of the conversation of MMA, in turn, can dilute the concentration of HEMA-TMS in mixture. Nevertheless, if the feeding rate was too slow, it would be difficult to form the gradient structure and tend to be block copolymer. As a whole, based on the simulated results, one knows that the feeding rate can not only control the structure of polymer chain but also affect the monomer conversion. Accordingly, the effects of feeding rate on the conversion and the instantaneous composition must be concurrently considered when one selects an appropriate feeding rate. The feeding rate data used by Matyjaszewski and coworkers[63] is a classical example.

Gradient Copolymers with Linear Gradient and Inverse Linear Gradient Composition

In this subsection, the effect of added monomer on the chain composition is predicted via the above model. For the linear gradient copolymers with a symmetric composition along chain, there are two approaches to be used to synthesize them with different direction of chain growth. For example, we can synthesize a normal linear gradient copolymer by initially charging all monomer (here is MMA) to the reactor and

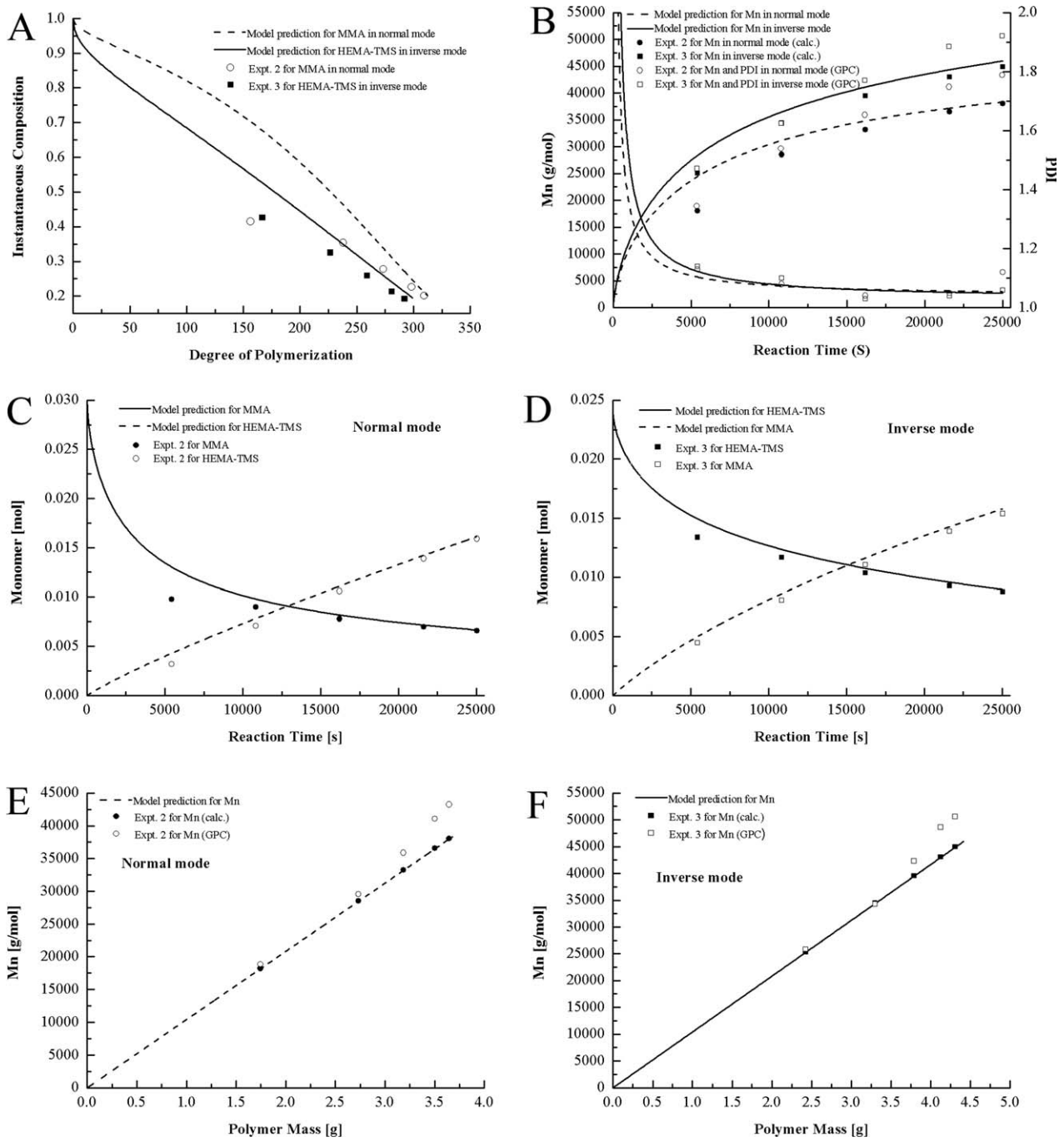

FIGURE 4 Comparison between model predictions and experimental data for the semibatch ATRP for producing linear (normal) and inverse linear (inverse) gradient copolymers: A instantaneous composition of poly(MMA-*grad*-HEMA-TMS) versus degree of polymerization, B molecular weight and polydispersity index versus reaction time, C and D monomer concentration versus reaction time, and E and F molecular weight versus polymer yield based on monomer conversion.

feeding the other monomer (here is HEMA-TMS) by the metering pump, the reactants and their recipes are listed in Table 9 (Expt. 2). If we charged all HEMA-TMS to the reactor and feed the MMA by the metering pump, an inverse linear gradient copolymer would be synthesized (Table 9, Expt. 3). Here, the model is used to investigate the synthesis of the linear gradient and inverse linear gradient copolymer at the similar experimental condition.

The experimental and simulated results are given in Figure 4. It is evident that the model predictions are in a good agreement with the experimental data. From Figure 4(A), the instantaneous composition of first monomer decreases continuously with the increase of the average polymer chain. For linear gradient copolymerization (normal mode), MMA is from 1 at the beginning of chain to 0.20 at the end and for inverse linear gradient copolymerization (inverse mode),

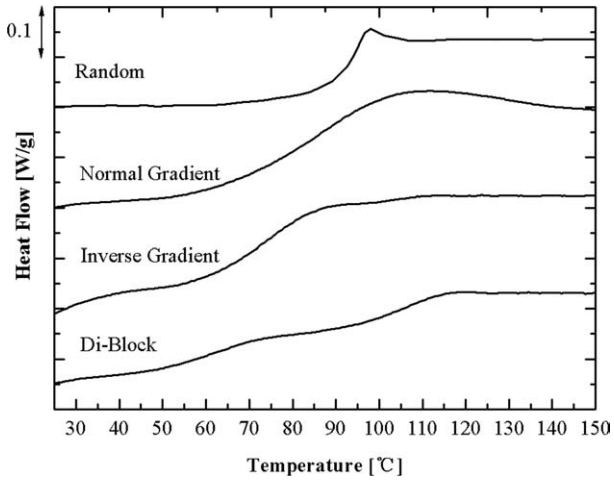

FIGURE 5 DSC heating curves for the MMA/HEMA copolymers with F_{HEMA} values from 0.22 to 0.25 (random copolymer, FHEMA = 0.25; block copolymer, FHEMA = 0.24; linear gradient copolymer FHEMA = 0.22; inverse linear gradient copolymer FHEMA = 0.52).

HEMA-TMS is from 1 to 0.19; however, the relationships between the instantaneous composition and degree of polymerization show that inverse mode is almost linear, which imply this pattern is more closed to ideal gradient composition. The composition along the chains deviates from the linear expression when the chains are short is also due to the slow initiator decomposition rate. Both the low PDI and the linear increase of Mn with reaction time shown in Figure 4(B) reflect the controllability of reaction. However, the influence of ideal conditions of simulation based on some assumptions on the deviation from simulation results remains at the end of reaction.

Figure 4(C or D) shows that both the two monomer conversions are quite different at the same reaction time, 78% for MMA and 28% for HEMA-TMS in normal mode at the end of reaction, while 46% for MMA and 63% for HEMA-TMS in inverse mode. It can be explained by the higher polymerization rate of MMA than HEMA-TMS and the feeding rate of second monomer. What is more, Figure 4(E and F) illustrate that, the relationship of Mn with polymer mass obvious with no great difference for normal and inverse mode. However, the Mn is up to 46,000 g mol^{-1} in inverse operation while it only reaches 38,000 g mol^{-1} in normal operation, that is to say, the total conversion has increased. Based on the above-simulated results, one can find that the inverse mode has a clear advantage over the normal mode in the monomer conversion and structure of polymer chains.

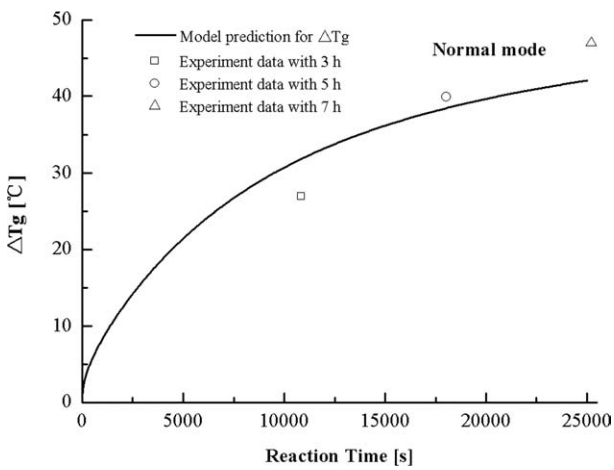

FIGURE 6 Comparison between model prediction and experimental data for the evolution of the T_g breadth in MMA/HEMA linear gradient copolymers as a function of reaction time.

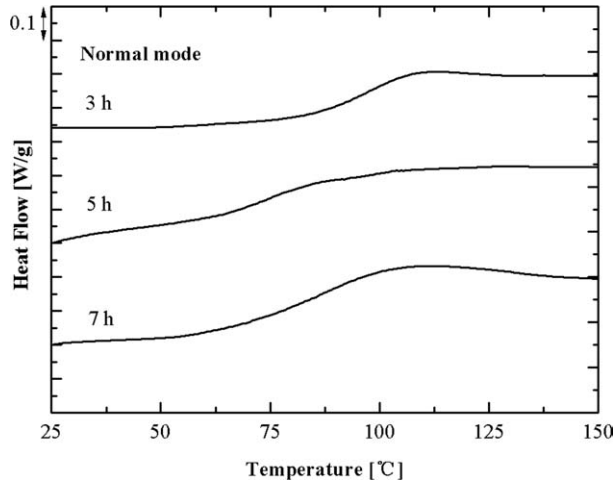

FIGURE 7 DSC heating curves for the MMA/HEMA linear gradient copolymers with different reaction time.

Thermal Properties of the Resulting Copolymers

The microstructure of linear gradient copolymer has been investigated through model and experiment. Gradient copolymers attract so many researchers to study mostly because of its intriguing thermal properties. Figure 5 provides the DSC

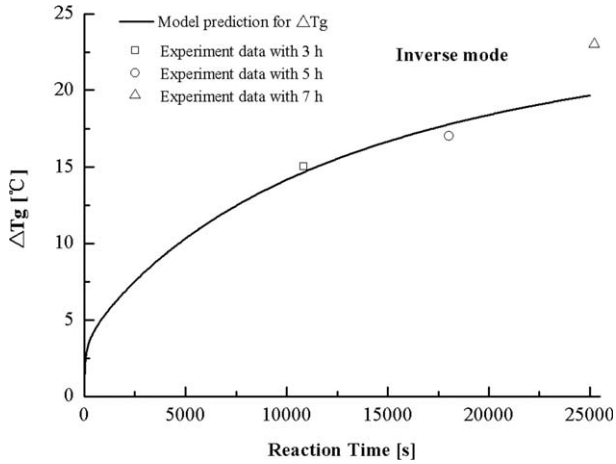

FIGURE 8 Comparison between model prediction and experimental data for the evolution of the T_g breadth in MMA/HEMA inverse linear gradient copolymers as a function of reaction time.

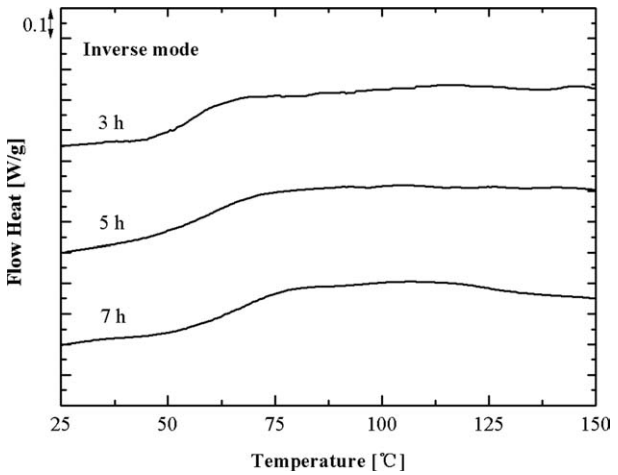

FIGURE 9 DSC heating curves for the MMA/HEMA inverse linear gradient copolymers with different reaction time.

heating curves for the MMA/HEMA copolymers with F_{HEMA} values from 0.22 to 0.25. It indicates that the random copolymer (Expt. 4; $F_{HEMA} = 0.25$) possesses a single, narrow T_g while the block copolymer (Expt. 5; $F_{HEMA} = 0.24$) possesses two discernable T_gs. In contrast, the linear gradient copolymer (Expt. 2; $F_{HEMA} = 0.22$) and inverse linear gradient copolymer (Expt. 3; $F_{HEMA} = 0.52$) exhibit one broad T_g.

Further study is used to understand the apparent relationship between the compositional gradient forms along the copolymer chain length and the evolution of T_g in the resulting gradient copolymers as a function of polymerization time.

Figures 6–9 illustrate the evolution of the T_g breadth ($\triangle T_g$) of the MMA/HEMA gradient copolymers as a function of polymerization time. From Figures 6–9, one knows that the breadth in T_g observed in the MMA/HEMA gradient copolymers is a direct consequence of the conversion and the composition gradient along the chain and the model prediction agrees well with the experimental results. In normal mode (Figs. 6 and 7), as the compositional gradient builds across the copolymer chain length during the semibatch reaction involving a gradual incorporation of HEMA into the copolymer, there is a gradual decrease in the T_g response at temperature approaching those of pure PHEMA without a loss of T_g response at higher temperature associated with the T_g of PMMA. Nevertheless, the contrary result can be found in the inverse mode (Figs. 8 and 9). For this result, it is explained by the presence of two factors, which can simultaneously affect T_g. The first one is the continuous increase in molecular weight with conversion would induce an increase in T_g of copolymers until reaching a plateau at high values where T_g becomes invariable, which can be rationalized by the reduction in free volume as the number of chain ends decreases with increasing molar mass; the second one is a composition variation causing a change in T_g.[65,66] In this case, both the Mns obtained by the normal mode and the inverse mode increase during the reaction process, which give rise to the increase of T_g. Simultaneously, there is a gradient composition with the enrichment of HEMA causing the decrease of T_g in the normal mode, while MMA causing the increase of T_g in the latter mode. Hence, combining the two factors, we can understand the results described in Figures 6–9.

However, Figures 6–9 also demonstrate that the changes of the breadths of T_g ($\triangle T_g$) with polymerization time for the two gradient copolymers are obviously different, the one produced by the normal mode is wider than the other produced by the inverse model. The Johnston theoretical model employed on this study can account for the phenomenon. According to the model function, one can find that the change rate of T_g becomes larger gradually with the increase of monomer mass fraction and the dyad distribution after some mathematical manipulations. In addition, we listed the T_g data (see Table 10) based on Figures 6–9. As a whole, various structural characteristics, such as composition, microstructure, and molecular weight, influence the glass transition temperature. Accordingly, it is indispensable to consider all these variables since they play an important role in understanding the relations between molecular structure and properties. The quantitative details on the change in T_g as a function of temporal development of the copolymer structure during the gradient copolymerization have been elaborated above. Therefore, our model can be applied to design the material with predetermined T_g.

CONCLUSIONS

A systematic study was carried out on the preparation of poly(MMA-*grad*-HEMA) with simultaneously tailor-made chain composition distribution and T_g through semibatch ATRP. The model was first validated by comparing simulation results with a classical reference data. Second, the model was used to investigate the effect of feeding rate on gradient composition and also guide the experimental synthesis of the poly(MMA-*grad*-HEMA) copolymer potentially as one of excellent damping materials. The model predicted the instantaneous composition, molecular weight, polydispersity index, monomer conversion, and polymer mass. The experimental data agreed well with the model prediction. Finally, The thermal properties of three different compositions copolymer samples has demonstrated that the gradient copolymers can possess distinctively broad T_gs in comparison with random and diblock copolymers. This difference in T_g reflected different morphologies that are determined by chain microstructural properties. The model prediction for T_g breadths

TABLE 10 Glass Transition Temperature Data for the Linear Gradient Copolymers Synthesized by Two Modes with Different Reaction Time

	Mode	Time (h)	T_{g0}[a] (°C)	T_{ge}[a] (°C)	$\triangle T_g$ (°C)
1	Normal	3	80	107	27
2	Normal	5	65	105	40
3	Normal	7	58	105	47
4	Inverse	3	55	70	15
5	Inverse	5	56	73	17
6	Inverse	7	55	78	23

[a] T_{g0} and T_{ge} are the starting and ending points of glass transition range, respectively.

exhibited by normal and inverse gradient copolymer evolved with the polymerization time was in accordance with the experimental results. It could be concluded that a comprehensive model for simultaneously predicting gradient copolymer microstructure and T_g value was presented.

ACKNOWLEDGMENTS

This work was supported by the National Natural Science Foundation of China (No. 20406016, 21076171). The authors really appreciate Xinyu Liu for DSC measuring in the college of materials, Xiamen University.

NOMENCLATURE

Capital and Small Letters

B_a	Adjustable parameter for activation
B_{da}	Adjustable parameter for deactivation
B_p	Adjustable parameter for chain propagation
B_{tr}	Adjustable parameter for chain transfer
B_{tc}	Adjustable parameter for combinative termination
B_{td}	Adjustable parameter for disproportional termination
C	Activator and catalyst at the lower oxidation state
C_i	Concentration of the species i in the reactor (mol m^{-3})
$C_{i,f}$	Concentration of the species i in the feed (mol m^{-3})
$k_{a,i}$	Activation rate constant for dormant chain with i-type of terminal unit (L mol^{-1} s^{-1})
$k_{da,i}$	Deactivation rate constant for radical with i-type of terminal unit (L mol^{-1} s^{-1})
$k_{p,ij}$	Chain propagation rate constant for monomer j adding to radical with i-type of terminal unit (L mol^{-1} s^{-1})
$k_{tr,ij}$	Chain transfer rate constant for monomer j adding to radical with i-type of terminal unit (L mol^{-1} s^{-1})
$k_{tc,ij}$	Combinative termination rate constant between radicals with i and j types of terminal unit (L mol^{-1} $s^{-1)}$
$k_{td,ij}$	Disproportional termination rate constant between radicals with i and j types of terminal unit (L mol^{-1} s^{-1})
$\overline{M_{n,i}}$	Number molecular weight of monomer i, (g mol^{-1})
M_i	Monomer i
$P_0 \cdot$	Primary radical
P_0X	Initiator
P_r	Dead chain with length r
P_s	Dead chain with length s
$P_{r,i} \cdot$	Propagating radical chain with length r and i-type of terminal unit
$P_{r,i}X$	Dormant chain with length r and i-type of terminal unit
r_i	Reactivity ratio of monomer i
$R_{p,i}$	Intrinsic propagation rate of the monomer i (mol m^{-3} s^{-1})
R_i	Intrinsic reaction rate of the species i (mol m^{-3} s^{-1})
R	Gas constant (J K^{-1} mol^{-1})
T	Temperature (K)
T_{gi}	Glass transition temperature of component i (K)
V_i	Volume of species i (m^3)
V	Volume of total system (m^3)
V_f	Volumetric feeding rate (m^3 s^{-1})
CX	Deactivator and catalyst at the higher oxidation state

Greek Letters

α_i	Thermal expansion coefficient of component i (L K^{-1})
τ_m	mth-order moment of dead chain
λ_i^m	mth-order moment of dormant chain with i-type of terminal unit
μ_i^m	mth-order moment of propagating radical with i-type of terminal unit
v_f	Free volume fraction (cm^3 s^{-1})
v_{f0}	Free volume fraction (cm^3 s^{-1})
ω_i	Mass fraction of monomer I in the copolymer
χ	Monomer conversion
ρ	Density of reaction mixture (kg m^{-3})
ρ_i	Density of component i (kg m^{-3})
ρ_f	Density of feeding materials (kg m^{-3})

Subscripts

0	Value at initial conditions
1	MMA
2	HEMA-TMS
m	Monomer
p	Polymer
S	Solvent

REFERENCES AND NOTES

1 Matyjaszewski, K.; Ziegler M. J.; Arehart, S. V.; Greszta, D.; Pakula, T. *J. Phys. Org. Chem.* **2000,** *13*, 775–786.

2 Beginn, U. *Colloid. Polym. Sci.* **2008,** *286*, 1465–1474

3 Karaky, K.; Billon, L.; Pouchan, C.; Desbrières, J. *Macromolecules* **2007,** *40*, 458–464.

4 Jakubowski, W.; Juhari, A.; Best, A.; Koynov, K.; Pakula, T.; Matyjaszewski, K. *Polymer* **2008,** *49*, 1567–1578.

5 Yuan, W.; Mok, M. M.; Kim, J.; Wong, C. L. H.; Dettmer, C. M.; Nguyen, S. T.; Torkelson, J. M.; Shull, K. R. *Langmuir* **2010,** *26*, 3261–3267

6 Medel, S.; Manuel García, J.; Garrido, L.; Quijada-Garrido, I.; París, R. *J. Polym. Sci. Part A: Polym. Chem.* **2011,** *49*, 690–700.

7 Zhao, Y.; Luo, Y. W.; Li, B. G.; Zhu, S. P. *Langmuir* **2011,** *27*, 11306–11315.

8 Milonaki, Y.; Kaditi, E.; Pispas, S.; Demetzos, C. *J. Polym. Sci. Part A: Polym. Chem.* **2012,** *50*, 1226–1237.

9 Khokhlov, A. R.; Berezkin, A. V.; Khalatur, P. G. *J. Polym. Sci. Part A: Polym. Chem.* **2004,** *42*, 5339–5353.

10 Lefebvre, M. D.; de la Cruz, M. O.; Shull, K. R. *Macromolecules* **2004,** *37*, 1118–1123.

11 Lefebvre, M. D.; Dettmer, C. M.; McSwain, R. L.; Xu, C.; Davila, J. R.; Composto, R. J.; Nguyen, S. T.; Shull, K. R. *Macromolecules* **2005,** *38*, 10494–10502.

12 Wang, R.; Li, W. H.; Luo, Y. W.; Li, B. G.; Shi, A. C.; Zhu, S. P. *Macromolecules* **2009,** *42*, 2275–2286.

13 Wong, C. L. H.; Kim, J.; Torkelson, J. M. *J. Polym. Sci. Part B: Polym. Phys.* **2007,** *45*, 2842–2849.

14 Mok, M. M.; Ellison, C. J.; Torkelson, J. M. *Macromolecules* **2011,** *44*, 6220–6226.

15 Kim, J.; Mok, M. M.; Sandoval, R. W.; Woo, D. J.; Torkelson, J. M. *Macromolecules* **2006,** *39*, 6152–6160.

16 Buzin, A. I.; Pyda, M.; Costanzo, P.; Matyjaszewski, K.; Wunderlich, B. *Polymer* **2002,** *43*, 5563–5569.

17 Mok, M. M.; Kim, J.; Torkelson, J. M. *J. Polym. Sci. Part B: Polym. Phys.* **2008,** *46*, 48–58.

18 Mok, M. M.; Kim, J.; Wong, C. L. H.; Marrou, S. R.; Woo, D. J.; Dettmer, C. M.; Nguyen, S. T.; Ellison, C. J.; Shull, K. R.; Torkelson, J. M. *Macromolecules* **2009,** *42*, 7863–7876.

19 Braunecker, W.A.; Matyjaszewski, K. *Prog. Polym. Sci.* **2007,** *32*, 93–146.

20 Hawker, C. J.; Bosman, A. W.; Harth, E. *Chem. Rev.* **2001,** *101*, 3661–3688.

21 Wang, L.; Broadbelt, L. J. *Macromolecules* **2009,** *42*, 7961–7968.

22 Matyjaszewski, K.; Xia, J. H. *Chem. Rev.* **2001,** *101*, 2921–2990.

23 Kamigaito, M.; Ando, T.; Sawamto, M. *Chem. Rev.* **2001,** *101*, 3689–3746.

24 Min, K.; Matyjaszewski, K. *J. Polym. Sci. Part A: Polym. Chem.* **2005,** *43*, 3616–3622.

25 Min, K.; Kwon Oh, J.; Matyjaszewski, K. *J. Polym. Sci. Part A: Polym. Chem.* **2007,** *45*, 1413–1423.

26 Chiefari, J.; Chong, Y. K.; Ercole, F.; Krstina, J.; Jeffrey, J.; Le, T. P. T.; Mayadunne, R. T. A.; Meijs, G. F.; Moad, C. L.; Moad, G.; Rizzardo, E.; Thang, S. H. *Macromolecules* **1998,** *31*, 5559–5562.

27 Perrier, S.; Takolpuckdee, P. *J. Polym. Sci. Part A: Polym. Chem.* **2005,** *43*, 5347–5393.

28 Rosen, B. M.; Percec, V. *Chem. Rev.* **2009,** *109*, 5069–5119.

29 Percec, V.; Popov, A. V.; Ramirez-Castillo, E.; Weichold, O. *J. Polym. Sci. Part A: Polym. Chem.* **2003,** *41*, 3283–3299.

30 Percec, V.; Guliashvili, T.; Ladislaw, J. S.; Wistrand, A.; Stjerndahl, A.; Sienkowska, M. J.; Monteiro, M. J.; Sahoo, S. *J. Am. Chem. Soc.* **2006,** *128*, 14156–14165.

31 Matyjaszewski, K. *Prog. Polym. Sci.* **2005,** *30*, 858–875.

32 Wang, L.; Broadbelt, L. *J. Macromol. Theory. Simul.* **2011,** *20*, 191–204.

33 Wang, R.; Luo, Y. W.; Li, B. G.; Sun, X. Y.; Zhu, S. P. *Macromol. Theory. Simul.* **2006,** *15*, 356–368.

34 Wang, R.; Luo, Y. W.; Li, B. G.; Zhu, S. P. *AIChE J* **2007,** *53*, 174–186.

35 Sun, X. Y.; Luo, Y. W.; Wang, R.; Li, B. G.; Liu, B.; Zhu, S. P. *Macromolecules* **2007,** *40*, 849–859.

36 Sun, X. Y.; Luo, Y. W.; Wang, R.; Li, B. G.; Zhu, S. P. *AIChE J.* **2008,** *54*, 1073–1087.

37 Zhao, Y.; Luo, Y. W.; Ye, C. H.; Li, B. G.; Zhu, S. P. *J. Polym. Sci. Part A: Polym. Chem.* **2009,** *47*, 69–79.

38 Ye, Y. S.; Schork, F. *J. Ind. Eng. Chem. Res.* **2009,** *48*, 10827–10839.

39 Hashimoto, T.; Tsukahara, Y.; Tachi, K.; Kawai, H. *Macromolecules* **1983,** *16*, 648–657.

40 Fevotte, G.; McKenna, T. F.; Santos, A. M. *Chem. Eng. Sci.* **1998,** *53*, 2241–2256.

41 Martín-Gomis, L.; Cuervo-Rodriguez, R.; Fernández-Monreal, M. C.; Madruga, E. L.; Fernández-García, M. *J. Polym. Sci. Part A: Polym. Chem.* **2003,** *41*, 2659–2666.

42 Liu, G. D.; Meng, Z. Y.; Wang, W.; Zhou, Y. L.; Zhang, L. C. *J. Phys. Chem. B* **2008,** *112*, 93–99.

43 Tonelli, A. E.; Jhon, Y. K.; Genzer, J. *Macromolecules* **2010,** *43*, 6912–6914.

44 D'hooge, D. R.; Reyniers, M. F.; Marin, G. B. *Macromol. React. Eng.* **2009,** *3*, 185–209.

45 Hamielec, A. E.; MacGregor, J. Polymer Reaction Engineering; Hanser Publishers: New York, **1983;** pp 21.

46 Morris, L. M.; Davis, T. P.; Chaplin, R. P. *Polymer* **2001,** *42*, 941–952.

47 Al-Harthi, M.; Soares, J. B. P.; Simon, L. C. *Macromol. React. Eng.* **2007,** *1*, 468–479.

48 Delgadillo-Vela'zquez, O.; Vivaldo-Lima, E.; Quintero-Ortega, I. A.; Zhu, S. P. *AIChE J.* **2002,** *18*, 2597–2508.

49 Johnston, N. W. *J. Macromol. Sci. Rev. Macromol. Chem.* **1976,** *14*, 214–250.

50 Fox, T. G. *Bull. Am. Phys. Soc.* **1956,** *1*, 123.

51 Beuermann, S.; Buback, M.; Davis, T. P.; Gilbert, R. G.; Hutchinson, R. A.; Olaj, O. F.; Russell, J.; Schweer, G. T.; Van Herk, A. M. *Macromol. Chem. Phys.* **1997,** *198*, 1545–1560.

52 Buback, M.; Kurz, C. H. *Macromol. Chem. Phys.* **1998,** *199*, 2301–2310.

53 Vivaldo-Lima, E.; Garcıa-Perez, R.; Celedon-Briones, O. *J. Rev. Soc. Quim. Mex.* **2003,** *47*, 22–33.

54 Goodner, M. D.; Lee, H. R.; Bowman, C. N. *Ind. Eng. Chem. Res.* **1997,** *36*, 1247–1252.

55 Walling, C. *J. Am. Chem. Soc.* **1949,** *71*, 1930–1935.

56 Brauna, D.; Czerwinski, W. K.; Tudos, F.; Kelenc, T.; Turcsanyi, B. *Die Angew Makromol. Chem.* **1990,** *118*, 209–219.

57 Hutchinson, R. A.; Aronson, M. T.; Richards, J. R. *Macromolecules* **1993,** *26*, 6410–6415.

58 Fedors, R. F. *J. Polym. Sci. Polym. Lett. Ed.* **1979,** *17*, 719–722.

59 Keramopoulos, A.; Kiparissides, C. *J. Appl. Polym. Sci.* **2003,** *88*, 161–176.

60 Yao, Y.; Xie, T.; Gao, Y. Handbook of Chemistry and Physics; Shanghai Scientific and Technical Publishers: Shanghai, **1985.**

61 Beers, K. L.; Gaynor, S. G.; Matyjaszewski, K.; Sheiko, S. S.; Moller, M. *Macromolecules* **1998,** *31*, 9413–9415.

62 Beers, K. L.; Boo, S.; Gaynor, S. G.; Matyjaszewski, K. *Macromolecules* **1999,** *32*, 5772–5776.

63 Borner, H. G.; Duran, D.; Matyjaszewski, K.; da Silva, M.; Sheiko, S. S. *Macromolecules* **2002,** *35*, 3387–3394.

64 Wang, J. L.; Grimaud, T.; Matyjaszewski, K. *Macromolecules* **1997,** *30*, 6507–6512.

65 Fernandez-García, M.; de la Fuente, J. L.; Fernandez-Sanz, M.; Madruga, E. L. *Macromol. Rapid. Commun.* **2001,** *22*, 1046–1052.

66 Cherifi. N.; Issoulie, A.; Khoukh, A.; Benaboura, A.; Save, M.; Derail, C.; Billon, L. *Polym. Chem.* **2011,** *2*, 1769–1777.